# Defibrillation of soft porous metal-organic frameworks with electric fields

**A. Knebel, B. Geppert, K. Volgmann, D. I. Kolokolov, A. G. Stepanov, J. Twiefel, P. Heitjans, Dirk Volkmer, J. Caro**

**Angaben zur Veröffentlichung / Publication details:**

Knebel, A., B. Geppert, K. Volgmann, D. I. Kolokolov, A. G. Stepanov, J. Twiefel, P. Heitjans, Dirk Volkmer, and J. Caro. 2017. "Defibrillation of soft porous metal-organic frameworks with electric fields." *Science* 358 (6361): 347–51. https://doi.org/10.1126/science.aal2456.



# Defibrillation of soft porous metal-organic frameworks with electric fields

**A. Knebel,[1]* B. Geppert,[1] K. Volgmann,[1] D. I. Kolokolov,[2,3] A. G. Stepanov,[2,3] J. Twiefel,[4] P. Heitjans,[1] D. Volkmer,[5] J. Caro[1]***

**Gas transport through metal-organic framework membranes (MOFs) was switched in situ by applying an external electric field (E-field). The switching of gas permeation upon E-field polarization could be explained by the structural transformation of the zeolitic imidazolate framework ZIF-8 into polymorphs with more rigid lattices. Permeation measurements under a direct-current E-field poling of 500 volts per millimeter showed reversibly controlled switching of the ZIF-8 into polar polymorphs, which was confirmed by x-ray diffraction and ab initio calculations. The stiffening of the lattice causes a reduction in gas transport through the membrane and sharpens the molecular sieving capability. Dielectric spectroscopy, polarization, and deuterium nuclear magnetic resonance studies revealed low-frequency resonances of ZIF-8 that we attribute to lattice flexibility and linker movement. Upon E-field polarization, we observed a defibrillation of the different lattice motions.**

Metal-organic frameworks (MOFs) are an emerging class of materials for gas separation, storage, and purification (*1*–*3*). However, MOFs lack the potential for sharp molecular sieving (*4*, *5*). For example, the MOF ZIF-8, with a pore diameter of 3.4 Å, allows the diffusion of molecules with larger kinetic diameters, such as *n*-hexane, benzene, and mesitylene (*6*), because of lattice flexibility. Indeed, MOFs are currently referred to as "soft porous crystals" (*7*). Recently, Bennett *et al.* presented a perspective on the interplay of different defects and disorders, with examples to prove that correct defect engineering enhances separation in MOFs (*8*). Many studies have been performed to reveal the flexibility mechanisms (*9*), but only one theoretical study has explored how to exploit the flexibility by means of electric fields (E-fields) (*10*).

Soft porosity is often related to breathing effects, shear deformation, and soft modes (*4*, *11*). Thermally triggered lattice motions have been linked to guest transport; for instance, in ZIF-8, the required energy for lattice movement is low, thus allowing mobility throughout the framework (*12*). Nonetheless, rigid MOFs also exist, such as HKUST-1, which contains fixed tridentate linker molecules in which only thermal lattice vibrations are observed (*13*). Terahertz spectroscopy of ZIF-8 revealed that linker rotation (*14*), shear deformation, and breathing and soft modes are thermally activated within the ZIF-8 lattice (*11*) and are omnipresent at room temperature. In previous studies, external E-fields influenced solutions (*15*) and dispersions (*16*) through ionic, dipolar, and electronic interactions.

We show that the stiffening of the ZIF-8 lattice through E-field polarization can reduce molecular transport and increase molecular sieving capability. The occurrence of lattice distortions is well known, but our understanding up to now is limited to ferro- or piezoelectric MOFs (*17*, *18*) or materials in general. In addition, phase changes in conductive coordination polymers under electric currents have been observed (*19*). However, we could not find any evidence via polarization measurements for the ferroelectric behavior of ZIF-8. We interpret the observed effects of ZIF-8 in an E-field as reversible phase transformations between the standard cubic symmetry and polarized monoclinic or triclinic space groups.

We observed signals for gating effects in ZIF-8; Devautour-Vinot *et al.* (*20*) and Frunza *et al.* (*21*) showed these effects in samples of UiO-66(Zr) and MOF-5, respectively, using dielectric spectroscopy and nuclear magnetic resonance (NMR) (*22*, *23*). The use of $^2$H NMR enabled measurement of very low frequencies of MOFs, uncovering distinctive bands attributed to lattice and linker motions. Because soft modes and shear deformation are acoustic phenomena at room temperature in ZIF-8 (*11*), we concluded that the lattice was stiffened through E-field polarization.

The linker motion in ZIF-8 was nonetheless affected by polarization; however, the activation barrier for complete alignment with the electric fields was very high, with a value of 49 to 60 kJ/mol. The highest contribution to the permittivity change originated from the ions (*24*). As the size selectivity and gas transport were switched by polarizing the ZIF-8 membrane, the selectivity for a propene-propane mixture increased. Thus, induced polarization is a nondestructive way to control gas transport through polycrystalline MOF layers. We show that reversible distortions of crystalline ZIF-8 membranes with E-fields can enhance molecular sieving. The complex mechanism underlying this effect was studied by DFT calculation, $^2$H NMR, dielectric spectroscopy and polarization, and gas permeation experiments; all techniques gave closely comparable results.

We used a polytetrafluoroethylene (PTFE) Wicke-Kallenbach permeation cell (Fig. 1, A and B) to perform E-field–assisted gas permeation measurements in situ on ZIF-8 membranes. [See (*25*) for concrete measurement protocols.] Scanning electron microscopy (SEM) of cross sections of the $Al_2O_3$- and $TiO_2$-supported ZIF-8 membrane layers and energy-dispersive x-ray spectroscopy (EDXS) were performed (Fig. 1, C and D) to determine the growth of the ZIF-8 layers, which were 1 μm and 20 μm thick, respectively. The MOF layers were well intergrown and did not infiltrate the supports.

Gas transport through the ZIF-8 membrane layers was measured, and the permeances (moles of gas per elapsed time, membrane area, and pressure difference) were in good accordance with literature values (Fig. 2, A to C) (*26*–*28*). The single-gas permeances of $H_2$, $CO_2$, and $CH_4$ on the 20-μm ZIF-8 membrane layer were measured with and without an in situ–applied E-field of 500 V/mm perpendicular to the MOF layer (Fig. 2A). Cycles of switching between the polymorphs were found—for example, for $CO_2$ using both the 20-μm and 1-μm ZIF-8 membranes (Fig. 2, C and E). ZIF-8 is known as one of the best membrane separation materials for propene and propane ($C_3H_6/C_3H_8$) (*27*, *28*). We separated such a mixture using the 1-μm ZIF-8 membrane (Fig. 2F). The separation factor for the $C_3H_6/C_3H_8$ mixture increased from 6 to 8 after applying the E-field.

Polarity reversal of the E-field yielded the same effect on gas transport. Because ZIF-8, as a flexible MOF, allows gate opening, shear deformation, and soft mode phase changes (*11*), HKUST-1, as a rigid MOF, was studied for comparison. As expected, no E-field influence on permeance through the HKUST-1 membrane could be observed (Fig. 2D), as no shear deformation or gate opening is possible (*13*). The permeances of the probe gases $H_2$, $CO_2$, and $CH_4$ through the HKUST-1 layer were in good agreement with reported values (*29*).

Given this difference, an ionic displacement and a stiffening of the network were considered to account for the switching of the gas transport through the ZIF-8 layer. As shown in Fig. 2, C and E, relaxation of the polarized ZIF-8 layer after removal of the E-field required ~1.5 hours in a continuous gas flow. In addition, at least for the 20-μm layer, the permeance values did not completely return to the original values, even after an additional 104 min. It is unclear why the 20-μm ZIF-8 layer did not return to the original separation performance, although the 1-μm thin layer did. Because we found that the permeances of all gases through the ZIF-8 membrane

[1]Institute of Physical Chemistry and Electrochemistry, Leibniz University Hannover, 30167 Hannover, Germany. [2]Boreskov Institute of Catalysis, Siberian Branch of Russian Academy of Sciences, Novosibirsk 630090, Russia. [3]Novosibirsk State University, Novosibirsk 630090, Russia. [4]Institute for Dynamic and Vibration Research, Leibniz University Hannover, 30167 Hannover, Germany. [5]Institute of Physics, Chair of Solid State and Materials Chemistry, Augsburg University, 86135 Augsburg, Germany.
*Corresponding author. Email: juergen.caro@pci.uni-hannover.de (J.C.); alexander.knebel@pci.uni-hannover.de (A.K.)

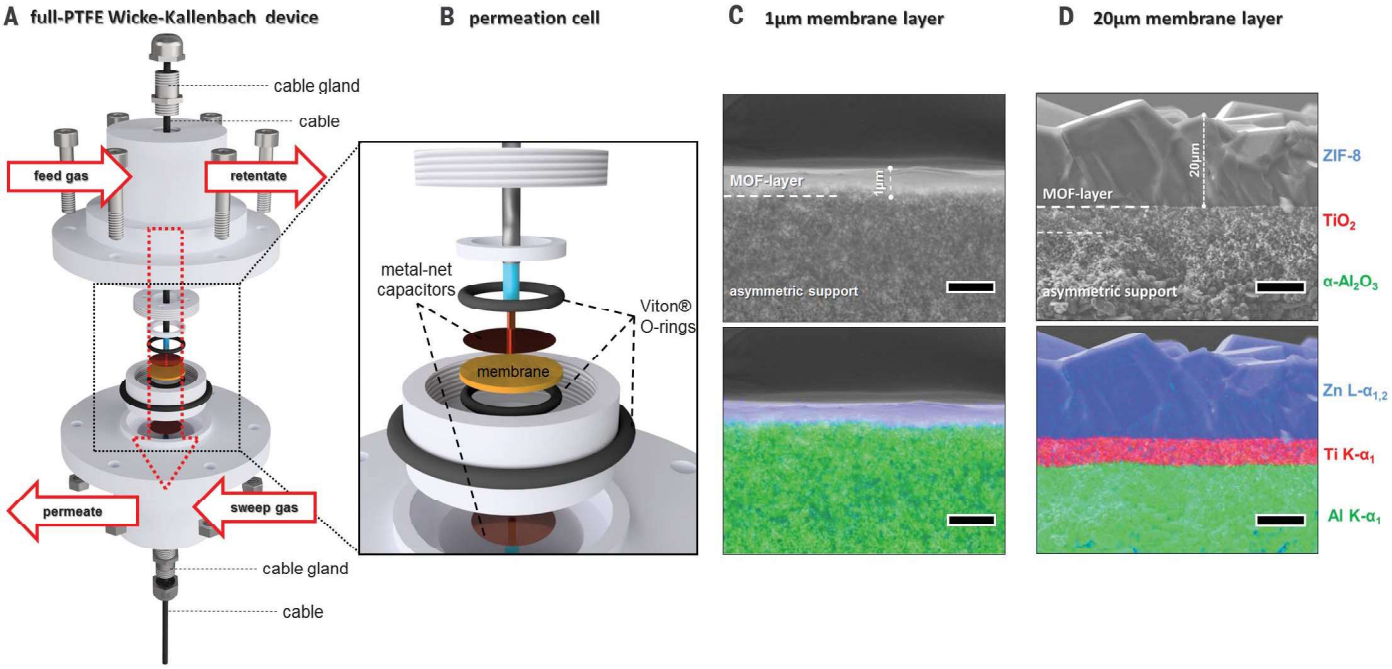


**Fig. 1. Design of the permeation cell and SEM of the ZIF-8 layer.** (**A** and **B**) The permeation cell for in situ E-field–controlled gas permeation measurements. (**C** and **D**) Cross-sectional SEM images of the ZIF-8 layer on a supporting ceramic. In (C), ZIF-8 of 1-µm thickness is grown on top of an $Al_2O_3$ supporting layer; in (D), ZIF-8 of 20-µm thickness is grown on top of a $TiO_2$ support. Scale bars, 2 µm (C), 10 µm (D). Color code of EDXS: blue, Zn L-$\alpha_{1,2}$; red, Ti K-$\alpha_1$; green, Al K-$\alpha_1$.

**Fig. 2. Single-gas permeation with an in situ applied E-field of 500 V/mm.** In (**A**), the in situ measured single-gas permeances for $H_2$, $CO_2$, and $CH_4$ are shown before applying an E-field, upon application of an E-field, and after relaxation. For all gases, the permeances decrease when an E-field of 500 V/mm is applied. When the E-field is switched off, after a relaxation time of ~100 min, the permeance instantaneously increases. (**B**) The ideal selectivities α (quotient of the ideal permeances $P_1/P_2$) were calculated from these single-gas permeances. The size selectivity decreases for smaller gases after polarization. (**C** and **E**) A demonstration of the in situ switching of $CO_2$ is shown in a plot of permeance versus time for the 20-µm membrane (C) and the 1-µm membrane (E). The $CO_2$ permeance decreases when the E-field is applied, remains in this state for approximately 100 min after shutdown of the E-field, and then recovers; the permeance of only the thin membrane recovers completely. (**D**) The single-gas permeances through the HKUST-1 membrane show no response to the E-field. (**F**) For propene-propane mixtures in ZIF-8, the real separation factor α (quotient of the real permeances $P_{propene}/P_{propane}$) increases upon E-field poling.

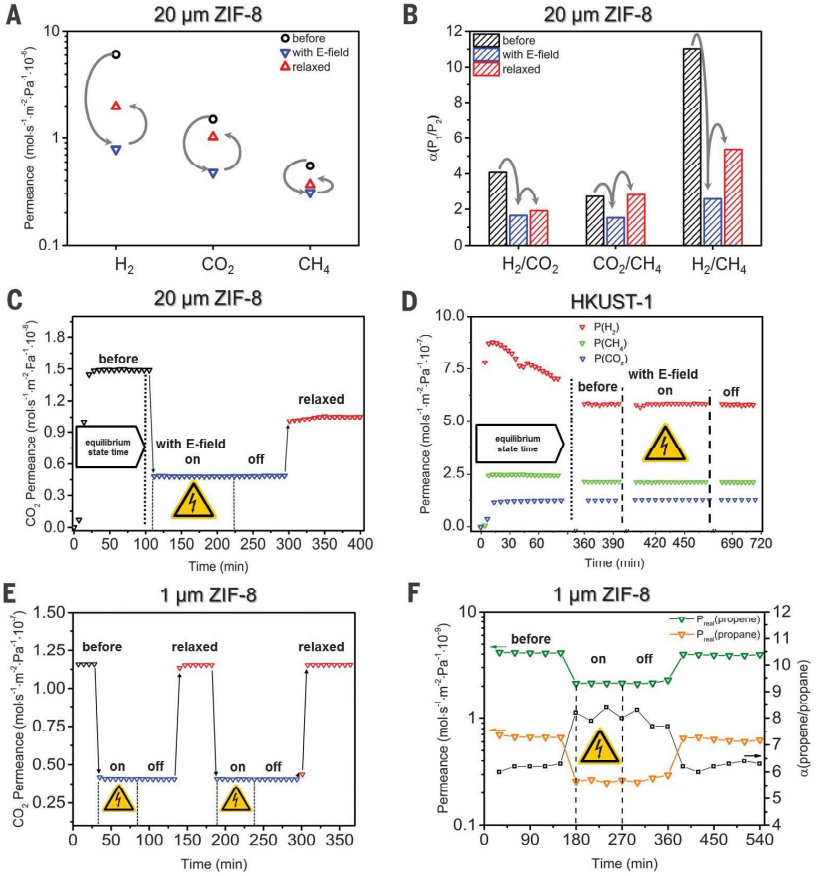

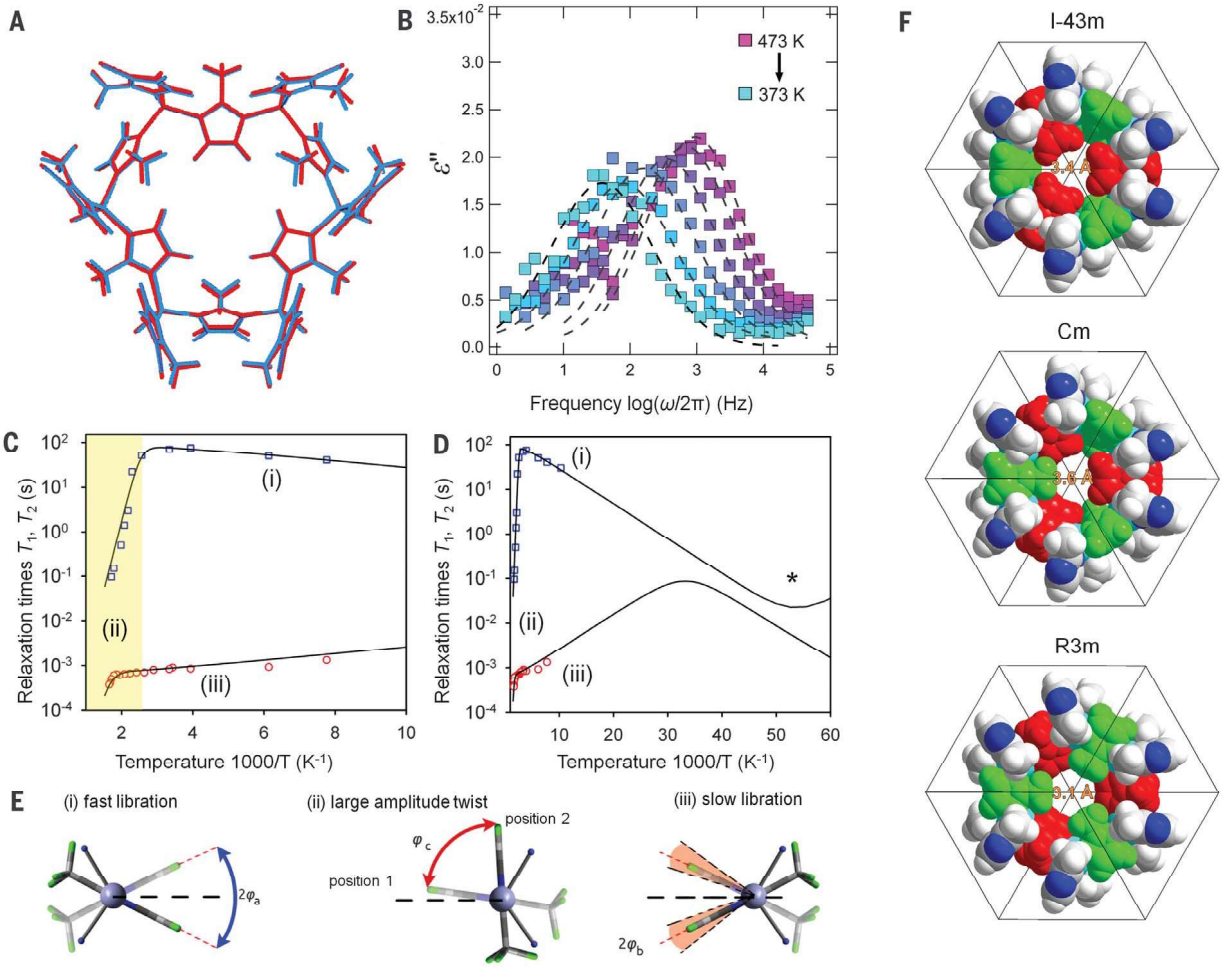


**Fig. 3. Simulated lattice; dielectric and $^2$H NMR spectroscopy of ZIF-8.** (**A**) Lattice overlay of the undisturbed ZIF-8 gate (blue) with the same lattice distorted by an external potential $U$ of the electric field strength (red), $|U|$ = 0.02 eV Å$^{-1}$ e$^{-1}$ in the ⟨111⟩ direction. See (*25*) for further experimental and theoretical XRD data. (**B**) Dielectric spectra of the imaginary part of the permittivity from 473 to 373 K, in steps of 20 K, over the frequency range $10^0$ to $10^5$ Hz with a voltage amplitude of 0.1 V. ZIF-8 shows a moment that responds to an AC E-field, as investigated by dielectric relaxation spectroscopy. (**C**) $^2$H NMR $T_1$ (squares) and $T_2$ (circles) relaxation curves of ZIF-8 as a function of temperature for the C-D group of the deuterated 2-mIM linker in ZIF-8; a very slow motion is observed in the region marked in yellow. The numerical simulation results are shown as solid lines. (**D**) The same data on an expanded temperature scale. (**E**) The evolution of $T_1$ and $T_2$ relaxation times with temperature, showing the presence of three main motions: (i) fast ($\tau_a$ ~ 1 ps) but relatively small-amplitude librations ($\varphi_a$ = ±30° at ~500 K) of the linker about the ZIF-8 window plane (*22*) and two much slower modes, (ii) and (iii). (**F**) A representation of the primitive cells of the ZIF-8 gate as a space-filling model of the different simulated polymorphs. Through deformation of the unit cell, the imidazolate linkers align (along with stiffening the network) and thereby avoid steric energy barriers of the bent unit cells.

decrease when the E-field is applied (Fig. 2A), this effect seems not to be beneficial at first glance. The ideal and real separation factors—calculated as the ratio of the single-gas or mixed-gas permeances—changed via the E-field–induced switching process. Figure 2A shows the single-gas permeation values for the small probe molecules $H_2$, $CO_2$, and $CH_4$; Fig. 2B shows the calculated ideal separation factors for the 20-μm layer before, during, and after applying an E-field of 500 V/mm. When applying the E-field, the selectivities and permeances were lower for the smaller molecules than for the larger ones (from $H_2$ and $CO_2$ to $CH_4$). A small widening of pores in the stiffened ZIF-8 could explain the lower selectivity for smaller gases and the higher selectivity for propene-propane mixtures. After the membranes relaxed, the original size selectivity was completely recovered only for the 1-μm ZIF-8 membrane.

As found by in situ gas permeation measurements, the MOF membrane was captured in a "switched" state after initial polarization for 1 to 2 hours, thus enabling the analysis of the "switched" ZIF-8. Before relaxation occurred, the ZIF-8 membrane was analyzed by x-ray diffraction (XRD) (fig. S1). The XRD analysis of the polarized ZIF-8 membrane revealed a uniform lattice strain. The XRD results were refined using TOPAS 4.1 with Rietveld refinement. The intensity changes and reflex shifts (fig. S1) are characteristic of uniform strain. [See (*25*) for lattice data for the polarized *R3m* and *Cm* polymorphs of ZIF-8.] Lattice distortion (fig. S1) shifted the reflexes to lower 2θ values, as depicted in a calculated lattice overlay in Fig. 3A.

Through ab initio density functional theory (DFT) calculations, we found that phase transformation changes the pore limiting diameter from 3.4 Å for cubic ZIF-8 to 3.6 Å for the *Cm* phase, which is the most dominant polarizable phase (figs. S1 and S6 to S8). The decreased permeances are caused by the stiffening in the ZIF-8 lattice, and we calculated a bulk modulus increase from 29 to 61 (*25*). This stiffening also influences the linker motion; linker rotations (Fig. 3D) are primarily inhibited, as seen in Fig. 3F. This stiffening originates from changes in the bond angles and different linker orientations for the individual polymorphs, shown as green and red linkers in Fig. 3F. However, the membrane remains intact, as previously confirmed by gas permeation measurements (Fig. 2, A to C), because destruction of the membrane would show gas breakthrough.

When an E-field is applied, a polymorphic phase transformation occurs (Fig. 3A and fig. S1). To further investigate these results, we performed dielectric spectroscopy analysis following procedures similar to those used with MOFs UiO-66 and MOF-5 (*20*, *21*). We applied dielectric spectroscopy to ZIF-8, as its linker 2-mIM is dipolar and rotatable; Fig. 3B shows the imaginary part $\varepsilon''$ of the permittivity $\varepsilon$ plotted versus frequency divided by $2\pi$. The dielectric response of ZIF-8 is evident by the temperature-dependent maxima in the permittivity, which shifted with increasing temperature to higher frequencies. The molecular resonances were excited by an AC voltage amplitude of 0.1 V. The temperature influence on the position of the $\varepsilon''$ maxima was investigated. The maxima correspond to a relaxation process, whose relaxation rate $\tau^{-1}$ is described by the relation $\omega\tau \approx 1$, where $\omega$ is the angular frequency of the AC voltage. The positions of the peak maxima shifted to higher frequencies as the temperature increased. This finding points to a thermally activated process, which could be described by an Arrhenius relation $\tau^{-1} = \tau_0^{-1} \exp(-E_A/kT)$, where $E_A$ is activation energy, $k$ is the Boltzmann constant, and $T$ is absolute temperature (*30*). The results were attributed to slow linker or lattice motions, which lie typically in the frequency region of 10 Hz to 10 kHz. The value of $E_A$ for the motion was 49 ± 6 kJ/mol and the prefactor $\tau_0^{-1}$ was $1.7 \times 10^9$ $s^{-1}$. Our findings are similar to those for other MOFs (*20*, *21*).

If our experimental findings corresponded to dipolar linker motion, a gate-opening-and-closing resonance would be observed. From the dielectric spectroscopy results, it can be assumed that a strong static DC E-field can align the dipoles. However, gate opening was calculated by DFT, and the required energy was too high for E-field alignment in our experiment (*25*). We performed $^2$H NMR to further investigate linker mobility (Fig. 3, C to E). The temperature dependences of the $T_1$ and $T_2$ relaxations for the deuterated C-D group of 2-mIM provide information about different motions exhibited by this linker. The $T_1$ relaxation is most sensitive to fast motions with rates comparable to $\omega_0$ (where $\omega_0/2\pi = 6.143 \times 10^7$ Hz is the NMR frequency of the $^2$H nuclei), whereas the $T_2$ relaxation can be very sensitive to slower modes. If the motion is an activated process, $\tau = \tau_0 \exp(E_A/RT)$ (where $\tau$ is the correlation time of the motion), the $T_1$ relaxation is characterized by a valley-like temperature dependence with a clear minimum (marked with an asterisk in Fig. 3D) corresponding to the temperature where $\tau^{-1} \approx \omega_0$. The slope of the relaxation curve outside the minimum is determined by the activation energy $E_A$ of this particular motion.

If there are multiple motions, then the effective correlation rate is formed by a linear combination of the characteristic correlation rates of the particular motions. As a result, if the characteristic correlation times and corresponding energy barriers are substantially different, the relaxation time temperature dependence curve contains multiple minima separated by regions of local maxima or curve bends. In the present case, the experimental temperature dependence showed exactly this situation. A very slow motion is shown in Fig. 3, C and D, in the region marked in yellow, characterized by a very large activation barrier of $E_A = 60 \pm 5$ kJ/mol and a pre-exponential factor of $\tau_0 \approx 10^{-10}$ s. We assume that this motion and that found by dielectric spectroscopy are the same. Geometrically, this finding can be interpreted as a large-amplitude $\varphi_c = 80°$ (±10°) twist of the linker relative to the ZIF-8 window plane at a rate of ~1 Hz to $5 \times 10^4$ Hz within the temperature range of 300 to 600 K, which is the same frequency range as that in dielectric spectroscopy. An illustration of the possible motions is shown in Fig. 3E. The stiffening of the network and the different pore diameters are pictured in Fig. 3F; from experiments, we found that *Cm* is the most dominant phase, which has a pore diameter of 3.6 Å with a much higher bulk modulus, thus stiffening and sharpening molecular sieving at 3.6 Å, optimal for propane-propene separation. It should be possible to further get ZIF-8 into the *R3m* phase with much higher fields, where the pore limiting diameter would be 3.1 Å (Fig. 3F) (*25*).

After studying the complex lattice polarization of ZIF-8, we investigated the ionic lattice response in detail. A piezo- or ferroelectric response of ZIF-8 was expected from the *I-43m* space group. From dielectric spectroscopy and NMR analysis, we know that the $Zn^{2+}$ ions of ZIF-8 contribute, because the activation barrier for dipolar linker motion is too high for the applied field (*24*). Using a 200-μm ZIF-8 single crystal as a capacitor (Fig. 4, A and B), we measured the

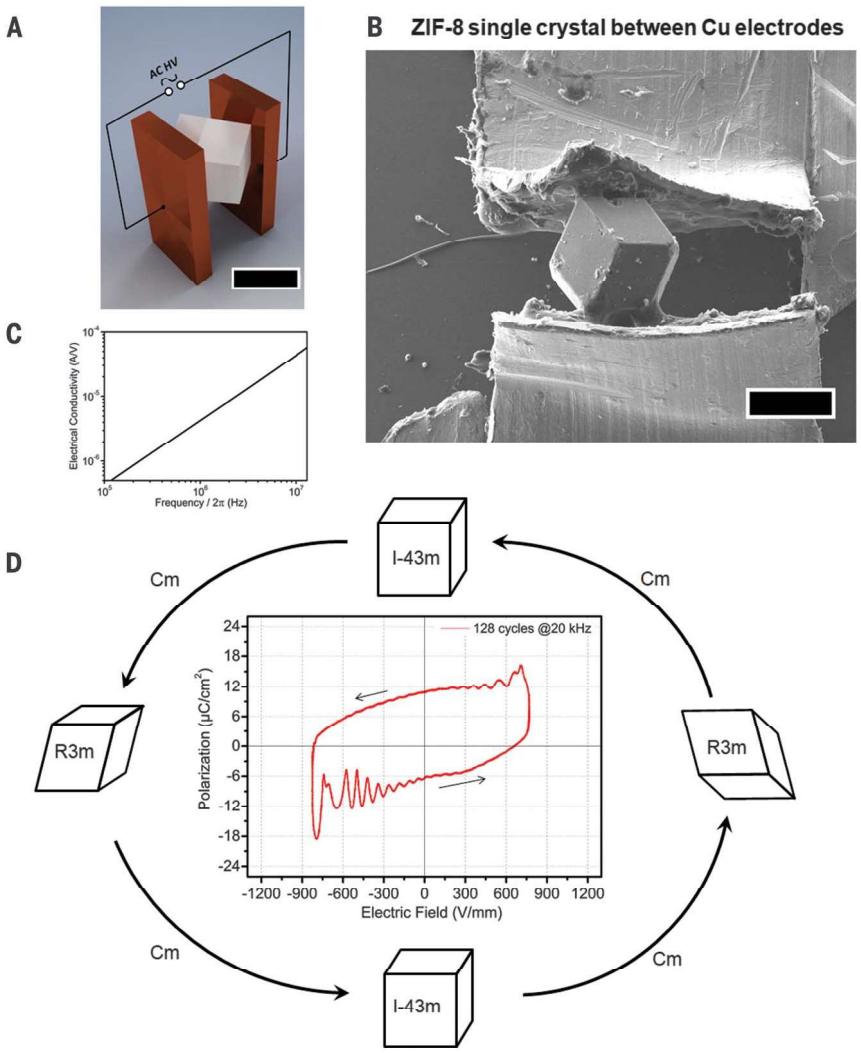


**Fig. 4. Ferro- and piezoelectric testing of a ZIF-8 single crystal.** (**A**) Wiring diagram of the ZIF-8 single-crystal polarization measurement. Scale bar, 200 μm. (**B**) SEM image of the crystal at 20 kV between segments of copper adhesive tape. The scale bar and the giant ZIF-8 crystal are 200 μm. (**C**) The electrical conductivity in the range of 1 to $10^7$ Hz. The results show a nearly linear curve, indicating the crystal to be almost an ideal insulator without a piezo- or ferroelectric response. (**D**) The polarization curve is measured at 20 kHz over the range of

frequency dependence of the electrical conductivity (Fig. 4C) and found a linear correlation, with no ferro- or piezoelectric response. In the polarization experiments (Fig. 4D), no ferroelectric hysteresis loop was observed, but "soft" lattice movement in the polarization direction is displayed as a broad curve, which is characteristic of soft materials. Without ferroelectric hysteresis, no evidence for the classical ferro- and piezoelectric ionic response of the lattice could be found. Thus, the lattice response found by XRD (fig. S1) can be assumed to be neither a classical ferroelectric response nor a piezoelectric response.

The interconnecting 2-methylimidazolate linker molecules in ZIF-8 play a critical role in gas separation. Adsorption and diffusion on MOFs are related to linker movements. Comparable to a defibrillation, we could reduce the framework fibrillation upon E-field polarization and stiffen the network. Here, the ZIF-8 lattice was polarized and a transformation from cubic to monoclinic and triclinic polymorphs, which led to marked changes in the gas permeation performance, occurred. However, with such low fields, the linkers were not completely aligned by the E-field. An estimated 30% of the MOF membrane layer was transformed into polymorphs with metastable ZIF-8 states as the lattice stiffened (fig. S1). This switching led to decreased separation selectivity for small molecules, such as $H_2$, $CO_2$, and $CH_4$. In contrast, for propene-propane mixtures, the stiffening of ZIF-8 improved molecular sieving, and the selectivity increased from 6 to 8. In the *Cm* space group, the limiting pore diameter of ZIF-8 changed from 3.4 to 3.6 Å in the polymorph. With higher E-fields than used in this paper, a full phase transformation should be possible, thus further enhancing gas separation. Other soft MOFs could be used as smart materials through electrical polarization. Force-field calculations show that a complete linker alignment cannot be reached by our weak E-fields, as the activation barrier lies between 49 and 60 kJ/mol. However, as shown through the polarization studies and impedance spectroscopy, a soft mode or shear deformation can be found, but no classical ferro- or piezoelectric response was observed in the lattice.

## REFERENCES AND NOTES


1. K. G. Ray *et al.*, *Chem. Mater.* **26**, 3976–3985 (2014).
2. B. Seoane *et al.*, *Chem. Soc. Rev.* **44**, 2421–2454 (2015).
3. A. W. Thornton *et al.*, *Energy Environ. Sci.* **5**, 7637 (2012).
4. G. Férey, C. Serre, *Chem. Soc. Rev.* **38**, 1380–1399 (2009).
5. L. Diestel, X. L. Liu, Y. S. Li, W. S. Yang, J. Caro, *Micropor. Mesopor. Mater.* **189**, 210–215 (2014).
6. D. I. Kolokolov, L. Diestel, J. Caro, D. Freude, A. G. Stepanov, *J. Phys. Chem. C* **118**, 12873–12879 (2014).
7. S. Horike, S. Shimomura, S. Kitagawa, *Nat. Chem.* **1**, 695–704 (2009).
8. T. D. Bennett, A. K. Cheetham, A. H. Fuchs, F.-X. Coudert, *Nat. Chem.* **9**, 11–16 (2016).
9. S. Henke, R. Schmid, J.-D. Grunwaldt, R. A. Fischer, *Chemistry* **16**, 14296–14306 (2010).
10. A. Ghoufi, K. Benhamed, L. Boukli-Hacene, G. Maurin, *ACS Cent. Sci.* **3**, 394–398 (2017).
11. M. R. Ryder *et al.*, *Phys. Rev. Lett.* **113**, 215502 (2014).
12. W. Morris, R. E. Taylor, C. Dybowski, O. M. Yaghi, M. A. Garcia-Garibay, *J. Mol. Struct.* **1004**, 94–101 (2011).
13. M. R. Ryder, B. Civalleri, G. Cinque, J. Tan, *CrystEngComm* **18**, 4303–4312 (2016).
14. D. Fairen-Jimenez *et al.*, *J. Am. Chem. Soc.* **133**, 8900–8902 (2011).
15. S. Murad, J. Lin, *Ind. Eng. Chem. Res.* **41**, 1076–1083 (2002).
16. N. Yanai, M. Sindoro, J. Yan, S. Granick, *J. Am. Chem. Soc.* **135**, 34–37 (2013).
17. W. Zhang, R. G. Xiong, *Chem. Rev.* **112**, 1163–1195 (2012).
18. D.-W. Fu, W. Zhang, R.-G. Xiong, *Dalton Trans.* **2008**, 3946–3948 (2008).
19. C. A. Fernandez *et al.*, *Sci. Rep.* **4**, 6114 (2014).
20. S. Devautour-Vinot *et al.*, *Chem. Mater.* **24**, 2168–2177 (2012).
21. S. Frunza *et al.*, *J. Phys. Chem. B* **114**, 12840–12846 (2010).
22. D. I. Kolokolov, A. G. Stepanov, H. Jobic, *J. Phys. Chem. C* **119**, 27512–27520 (2015).
23. A. K. Rizos, J. Alifragis, K. L. Ngai, P. Heitjans, *J. Chem. Phys.* **114**, 931–934 (2001).
24. S. Eslava *et al.*, *Chem. Mater.* **25**, 27–33 (2013).
25. See supplementary materials.
26. H. Bux *et al.*, *J. Am. Chem. Soc.* **131**, 16000–16001 (2009).
27. A. J. Brown *et al.*, *Science* **345**, 72–75 (2014).
28. H. T. Kwon, H.-K. Jeong, *Chem. Commun.* **49**, 3854–3856 (2013).
29. J. Nan, X. Dong, W. Wang, W. Jin, N. Xu, *Langmuir* **27**, 4309–4312 (2011).
30. P. Heitjans, J. Kärger, Eds., *Diffusion in Condensed Matter—Methods, Materials and Models* (Springer, ed. 2, 2005).


## ACKNOWLEDGMENTS


Supported by the Deutsche Forschungsgemeinschaft in the priority program SPP 1928 COORNETs (Coordination Networks: Building Block for Functional Systems), grant no. CA 147/20-1 (J.C.), VO 829/12-1 (D.V.), Russian Science Foundation project no. 17-73-10135 (D.I.K.), Russian Academy of Sciences project no. 0303-2016-0003 for the Boreskov Institute of Catalysis (A.G.S.), and by a Niedersachsen Professorship (P.H.). All data are reported in the main paper and supplement. The authors declare no competing financial interest.


## SUPPLEMENTARY MATERIALS

www.sciencemag.org/content/358/6361/347/suppl/DC1
Materials and Methods
Supplementary Text
Figs. S1 to S8
Tables S1 and S2
References (*31*–*41*)
Crystallographic Information Files